Progress In Electromagnetics Research, Vol. 131, 135–152, 2012

A SIMPLE LOCAL APPROXIMATION FDTD MODEL OF SHORT APERTURES WITH A FINITE THICKNESS

R. Xiong[1], B. Chen[1, *], Y.-F. Mao[1], B. Li[2], and Q.-F. Jing[2]

[1]National Key Laboratory on Electromagnetic Environment and Electro-optical Engineering, PLA University of Science and Technology, Nanjing, Jiangsu 210007, China

[2]PLA University of Science and Technology, Nanjing, Jiangsu 210007, China

Abstract—This paper brings forward a simple local approximation finite-difference time-domain (FDTD) method for the analysis of short apertures with a finite thickness. By applying the equivalence principle together with a simple local approximation, the varying field distribution is accurately derived. The updating equations for the slot field can be derived by casting the field distributions into the contour paths containing the apertures. The method has been applied to two problems and the results are compared with the high-resolution standard FDTD simulation results and the measurement results. The accuracy of the proposed method is verified from the comparison of both the field distribution and the time-domain and frequency-domain slot coupling results. It is demonstrated that the local approximation is highly efficient and timesaving, and the present method is stable, numerically and computationally efficient.

1. INTRODUCTION

The finite-difference time-domain (FDTD) method has been widely applied in solving many types of electromagnetic scattering problems [1–8]. It possesses the advantages of simple and accurate implementation for relatively complex problems. A disadvantage of the FDTD method is that significant computational resources are cost for modeling an electrically small object. Radiation from thin-slots falls into this category because the slot thickness and width can be much smaller than a desirable grid dimension.

Received 22 July 2012, Accepted 23 August 2012, Scheduled 5 September 2012

* Corresponding author: Bin Chen (emcchen@163.com).

Radiation from slots and seams is of greater concern as the speed of the electronic designs increases [9–17]. Thin-slot formalism permits inclusion of conducting plates with arbitrarily narrow apertures or gaps without requiring any corresponding need to reduce the cell size to the gap width or depth for the FDTD analysis. Several Thin-slot formalisms have been proposed in the literature [18–23]. However, they are mostly for apertures having zero thickness, and when slots with finite thickness are involved, only the hybrid thin-slot algorithm (HTSA) can be effective [22]. Nevertheless, the HTSA is complicated to implement, sensitive and susceptible to instability [24].

In this work, the equivalence principle is used to decouple the aperture coupling into three parts by placing the equivalent magnetic current sheets on the two sides of the slot. With the high-resolution local approximation, the equivalent magnetic current sheets are obtained with the modified slot width. Then the field near the slot can be derived from the conformal mapping technique together with the linear distribution assumption. The field distribution is fully cast into the integral equations to yield the coefficients for the FDTD updating algorithm.

To provide a benchmark for comparison, both the high-resolution FDTD simulation of the completely computational domain and the measured results are included. The accuracy of the proposed method is verified from the comparison of the varying field distribution and the time-domain and frequency-domain slot coupling results. It is demonstrated that the local approximation is highly efficient while timesaving, and the method presented here is stable, numerically and computationally efficient.

2. ANALYSIS OF THE FIELD DISTRIBUTION NEAR THE SLOT

Without losing generality, the coupling of a short aperture with a finite thickness between two regions, called region a and region b, is studied, as shown in Fig. 1(a). The thickness of the wall where the slot located is d, and the slot width is w, length is L. The slot is illuminated by a normally incident, x-polarized Gaussian plane wave in the form of

$$E_x = \exp\left[-\frac{4\pi(t-t_0)^2}{\tau^2}\right] \tag{1}$$

where $\tau = 0.2\,\text{ns}$, $t_0 = 0.6\,\text{ns}$, and the efficient frequency spectrum of the pulse ranges from DC to 10 GHz.

The equivalence principle [25, Sections 3–5] is used to divide the original problem into three decoupled parts, called region a, b, and c,

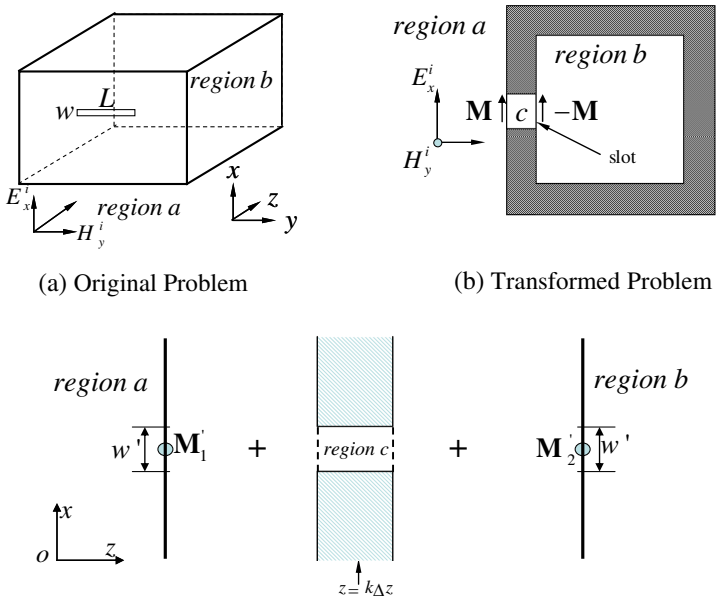

(a) Original Problem

(b) Transformed Problem

(c) Equivalent Transformed Problem

Figure 1. Transforming the coupling of the aperture with a finite thickness to the equivalent problem. The depth of the conductor in (1) and (2) of (c) is zero.

by placing equivalent magnetic current sheets on the opposite sides of the slot, as shown in Fig. 1(b). To get the field distribution near the slot, Fig. 1(b) is transformed to Fig. 1(c) with the equivalent magnetic current sheets and the equivalent slot width $w' = vw$, where $v \leq 1$. The field distribution in region c of Fig. 1(c) is obtained from the high-resolution local approximation, as introduced in Section 3.

To transform Fig. 1(b) to Fig. 1(c), two equivalence principles are used. One equivalence principle is that the slot voltage of both (b) and (c) is the same, or that magnetic current of (b) equals to (c)

$$\int_{-w/2}^{w/2} \mathbf{M}_{1,2} \cdot d\mathbf{x} = \int_{-w'/2}^{w'/2} \mathbf{M}'_{1,2} \cdot d\mathbf{x} \tag{2}$$

Another equivalence principle is that the electric field component E_x in region c of Fig. 1(c) equals that of Fig. 1(b)

$$E_x^h(x, y, z) = E_x(x, y, z) \tag{3}$$

where $E_x^h(x, y, z)$ is the field obtained by the local approximation in Section 3.

In region b of Fig. 1(c), the field is induced by the equivalent magnetic current $\mathbf{M}'_2$, which can be analytically expressed from conformal mapping technique with the equivalent slot width w'. While in region a, the field near the aperture can be decoupled into two parts. One part is induced by the magnetic current $\mathbf{M}'_1$. The other part is produced by the incident wave with the slot covered by an electric conductor, which can be obtained from a linear approximation [23]. In region c, the field is obtained from the high-resolution local approximation.

Therefore, the distribution the electric field component E_x and the magnetic field component H_z in the z direction can be written respectively as

$$E_x\left(i+\frac{1}{2},j,z\right)=\begin{cases}E'_{xa}+E^s_x, & ((k-1)\Delta_z<z\le -d/2)\\ E^h_x\left(i+\frac{1}{2},j,z\right), & (-d/2<z<d/2)\\ E'_{xb}, & (d/2<z\le (k+1)\Delta_z)\end{cases} \tag{4}$$

$$H_z\left(i+\frac{1}{2},j+\frac{1}{2},z\right)=\begin{cases}H'_{za}, & ((k-1)\Delta_z<z\le -d/2)\\ H^h_z\left(i+\frac{1}{2},j,z\right), & (-d/2<z<d/2)\\ H'_{zb}, & (d/2<z\le (k+1)\Delta_z)\end{cases} \tag{5}$$

where E'_{xa}, E'_{xb}, H'_{xa}, H'_{xb} are the fields induced by the magnetic currents, and E^h_x, H^h_z are obtained from the high-resolution local approximation. E^s_x is the field produced by the incident wave with the aperture covered by an electric conductor in the region a, Δ_z the grid dimension of the main computation in the z direction, and the point $[(i+\frac{1}{2})\Delta_x, j\Delta_y, k\Delta_z]$ is at the center of the slot.

In Fig. 1(b), the magnitude of the magnetic current density $\mathbf{M}_{1,2}$ can be obtained from numerical results, but its distribution is complicated and it is hard to be analytically expressed. Because the distribution of the equivalent magnetic current sheets at $z=k\Delta_z\pm d/2$ is different from that having zero thickness, the field induced by the magnetic current in region a and region b is not the same as that having zero thickness. Here, the parameter d is the slot depth, as defined in Fig. 2.

However, the distribution of the magnetic current and its radiation field can be analytically obtained for apertures having zero thickness. Therefore, transform the problem (b) to (c) with the modified equivalent slot width w', and then the field distribution in region a and region b can be gained analytically.

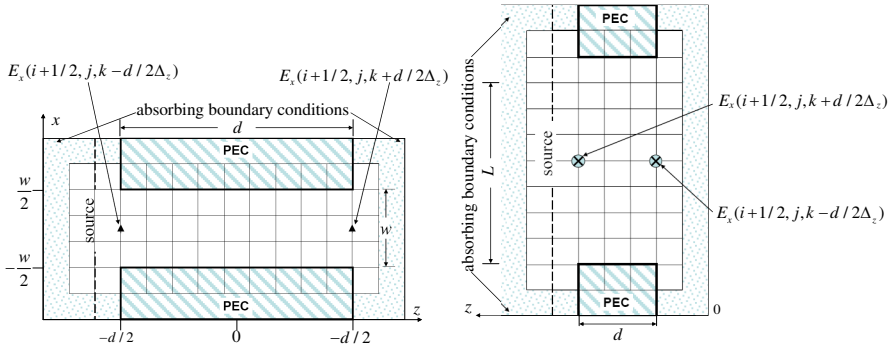

Figure 2. Computational area of the three-dimensional modeling of the aperture area.

In Fig. 1(c), it is assumed

$$E_x(x, j, k \pm d/2\Delta_z) = E_x^h\left(i+\frac{1}{2}, j, k \pm d/2\Delta_z^h\right) f(x), \quad \left|x-\left(i+\frac{1}{2}\right)\Delta_x\right| \le w/2 \tag{6}$$

where Δ_z^h is the spacial size of the cell of the local approximation, $f(x)$ is the normalized field distribution function obtained from the high-resolution local approximation in Section 3.

$$f(x) = \frac{E_x^h(x, j, k \pm d/2\Delta_z^h)}{E_x^h\left(i+\frac{1}{2}, j, k \pm d/2\Delta_z^h\right)} \tag{7}$$

It is worth to note that when the slot depth is tending to zero, $f(x)$ can be derived from [23, Eq. (10)] as

$$f(x)|_{d=0} = \frac{w/2}{\sqrt{(w/2)^2 - \left(\left(i+\frac{1}{2}\right)\Delta_x - x\right)^2}}, \quad \left|x-\left(i+\frac{1}{2}\right)\Delta_x\right| \le w/2 \tag{8}$$

The field deduced by the magnetic current of Fig. 1(c) in region a and region b along x can be analytically given as [23]

$$E_x'(x, j, k \pm d/2\Delta_z) = \frac{w' E_x'\left(i+\frac{1}{2}, j, k \pm d/2\Delta_z\right)}{2\sqrt{(w/2)^2 - \left(\left(i+\frac{1}{2}\right)\Delta_x - x\right)^2}} \tag{9}$$

Substituting (6) and (9) into (2), we can get

$$E_x^h\left(i+\frac{1}{2},j,k\pm d/2\Delta_z^h\right)\int_{-w/2}^{w/2}f(x)dx = \frac{w'}{2}E_x'\left(i+\frac{1}{2},j,k\pm d/2\Delta_z\right)\int_{-w'/2}^{w'/2}\frac{dx}{\sqrt{(w'/2)^2-\left(\left(i+\frac{1}{2}\right)\Delta_x-x\right)^2}} \quad (10)$$

Together with (3) and then the following can be derived

$$w' = \frac{2\int_{-w/2}^{w/2}f(x)dx}{\int_{-w'/2}^{w'/2}\frac{dx}{\sqrt{(w'/2)^2-\left(\left(i+\frac{1}{2}\right)\Delta_x-x\right)^2}}} = \nu w \quad (11)$$

where v is the equivalent slot width coefficient

$$\nu = \frac{\frac{1}{w}\int_{-w/2}^{w/2}f(x)dx}{\int_{-w'/2}^{w'/2}\frac{dx}{\sqrt{(w'/2)^2-\left(\left(i+\frac{1}{2}\right)\Delta_x-x\right)^2}}} = \frac{2}{\pi w}\int_{-w/2}^{w/2}f(x)dx \quad (12)$$

The integral $\int_{-w/2}^{w/2}f(x)dx$ can be obtained from the complex Simpson formula with the field given by the high-resolution local approximation in Section 3.

The electric field component E_x' produced by the equivalent magnetic current of Fig. 1(c) in region b can be derived from conformal mapping technique [23]

$$E_x'\left(i+\frac{1}{2},j,z\right) = \frac{w'/2}{\sqrt{(w'/2)^2+((k\Delta_z+d/2)-z)^2}}E_x^h\left(i+\frac{1}{2},j,k+d/2\Delta_z^h\right) \quad (13)$$

Together with the equivalent slot width coefficient (12), we can get the field distribution induced by the equivalent magnetic currents in region a and region b of Fig. 1(a)

$$E_x'\left(i+\frac{1}{2},j,z\right) = E_x^h\left(i+\frac{1}{2},j,k\pm d/2\Delta_z^h\right)\frac{\nu w/2}{\sqrt{(\nu w/2)^2+((k\Delta_z\pm d/2)-z)^2}}, \quad d/2\le|z-k\Delta_z|\le\Delta_z \quad (14)$$

To get the E_x^s distribution in (4), a linear approximation is occupied [23] while the field component E_x^s is zero at $z=k\Delta_z-d/2$

$$E_x^s\left(i+\frac{1}{2},j,z\right) = \frac{(k\Delta_z-d/2)-z}{\Delta_z-d/2}E_{xm}^s, \quad (d/2\le k\Delta_z-z\le\Delta_z) \quad (15)$$

Exploiting the same analogy as [23, Eqs. (14)–(16)], E^s_{xm} can be derived, and then (15) can be converted to

$$E^s_x\left(i+\frac{1}{2},j,z\right)=\frac{(k\Delta_z-d/2)-z}{\Delta_z-d/2}\left(E_x\left(i+\frac{1}{2},j,k-1\right)-E_x\left(i+\frac{1}{2},j,k+1\right)\right), \quad (d/2\le k\Delta_z-z\le\Delta_z) \quad (16)$$

Substituting (14) and (16) into (4), we can get the E_x distribution of Fig. 1(a)

$$E_x\left(i+\frac{1}{2},y,z\right) = \begin{cases} \left(E_x\left(i+\frac{1}{2},j,k-1\right)-E_x\left(i+\frac{1}{2},j,k+1\right)\right)\dfrac{(k\Delta_z-d/2)-z}{\Delta_z-d/2} \\ +E^h_x\left(i+\frac{1}{2},j,k-d/2\Delta^h_z\right)\dfrac{\nu w/2}{\sqrt{(\nu w/2)^2+((k\Delta_z-d/2)-z)^2}}, \\ \qquad (-\Delta_z\le z-k\Delta_z\le -d/2,\ |y-j\Delta_y|\le\Delta_y/2) \\ E^h_x\left(i+\frac{1}{2},j,k\right),\ (-d/2<z-k\Delta_z<d/2,\ |y-j\Delta_y|\le\Delta_y/2) \\ E^h_x\left(i+\frac{1}{2},j,k+d/2\Delta^h_z\right)\dfrac{\nu w/2}{\sqrt{(\nu w/2)^2+(z-(k\Delta_z+d/2))^2}}, \\ \qquad (d/2\le z-k\Delta_z\le\Delta_z,\ |y-j\Delta_y|\le\Delta_y/2) \end{cases} \quad (17)$$

and also the H_z distribution

$$H_z\left(i+\frac{1}{2},j,z\right) = \begin{cases} H^h_x\left(i+\frac{1}{2},j,k+d/2\Delta^h_z\right)\dfrac{\nu w/2}{\sqrt{(\nu w/2)^2+((k\Delta_z-d/2)-z)^2}}, \\ \qquad (-\Delta_z\le z-k\Delta_z\le -d/2,\ |y-j\Delta_y|\le\Delta_y/2) \\ H^h_z\left(i+\frac{1}{2},j,z\right),\ (-d/2<z-k\Delta_z<d/2,\ |y-j\Delta_y|\le\Delta_y/2) \\ H^h_z\left(i+\frac{1}{2},j,k-d/2\Delta^h_z\right)\dfrac{\nu w/2}{\sqrt{(\nu w/2)^2+(z-(k\Delta_z+d/2))^2}}, \\ \qquad (d/2\le z-k\Delta_z\le\Delta_z,\ |y-j\Delta_y|\le\Delta_y/2) \end{cases} \quad (18)$$

It is worth to note that when the slot depth d is tending to zero, the coefficient ν is tending to 1, and the field distribution (17) and (18) are the same as [23, Eq. (17)] and [23, Eq. (12)].

3. LOCAL APPROXIMATION OF THE SLOT AREA

To get the E_x^h and H_z^h distribution in region c of Fig. 1(c) without resulting in huge computational resources, the three-dimensional high-resolution simulation of the slot area is needed, as shown in Fig. 2. To model the slot area with the minimal memory usage, the source is induced at the plane one cell away from the slot plane. By the high-resolution approximation of the local area shown in Fig. 2, we can get the E_x^h and H_z^h variation in the aperture area, which can be used to yield integral coefficients respectively as

$$\kappa_{Ex}^z = \frac{\Delta_z^h \sum\limits_{z=-d/2\Delta_z^h}^{d/2\Delta_z^h} E_x^h\left(i+\frac{1}{2},j,z\right)}{E_x^h\left(i+\frac{1}{2},j,k\right)} \tag{19}$$

$$\kappa_{Hz}^z = \frac{\Delta_z^h \sum\limits_{z=-d/2\Delta_z^h}^{d/2\Delta_z^h} H_z^h\left(i+\frac{1}{2},j+\frac{1}{2},z\right)}{H_z^h\left(i+\frac{1}{2},j+\frac{1}{2},k\right)} \tag{20}$$

$$\kappa_{Hz}^{xy} = \frac{\Delta_y^h \sum\limits_{y=j\Delta_y^h}^{(j+1)\Delta_y^h} \sum\limits_{x=-w/2\Delta_x^h}^{w/2\Delta_x^h} H_z^h(x,y,k)}{w\Delta_y H_z^h\left(i+\frac{1}{2},j+\frac{1}{2},k\right)} \tag{21}$$

where κ_{Ex}^z and κ_{Hz}^z are the field distribution coefficient of the field components E_x^h and H_z^h in the slot depth, κ_{Hz}^{xy} is the field distribution coefficient in the cell at the slot edge, Δ_y, Δ_z is the dimension of a cell of the main computation, E_x^h, Δ_x^h and Δ_z^h are the electric field and the cell size of the local approximation, as shown in Fig. 2.

To reduce the local approximation time, we monitored the time history of the coefficient ν. Fig. 3 is the time history of the coefficient ν for the case $w = 1.67\,\text{mm}$, $d = 3.33\,\text{mm}$, $L = 20\,\text{mm}$.

It can be seen that the coefficient ν is almost constant versus time, and the singularity occurs only when the electrical field E_x^h is near zero. The same conclusions can be got from the observation of the other coefficients κ_{Ex}^z, κ_{Hz}^z, and κ_{Hz}^{xy}. Therefore, it is not needed to carry out the local approximation synchronously with the main computation, and a short pulse can be effective and the local approximation can be terminated when the slot field is varying continually. For example, when the electric field component E_x^h at the center of the slot reaches 10% of its peak value, the local approximation can be terminated and the coefficients can be obtained from the numerical integral.

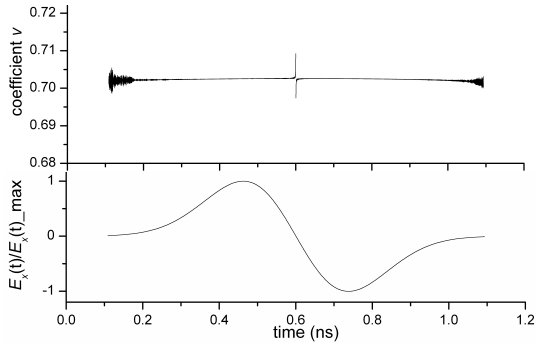

Figure 3. Time history of the coefficient v versus time. The time history of the normalized electric field component $E_x^h(i+\frac{1}{2}, j, k \pm d/2\Delta_z^h)$ is also presented.

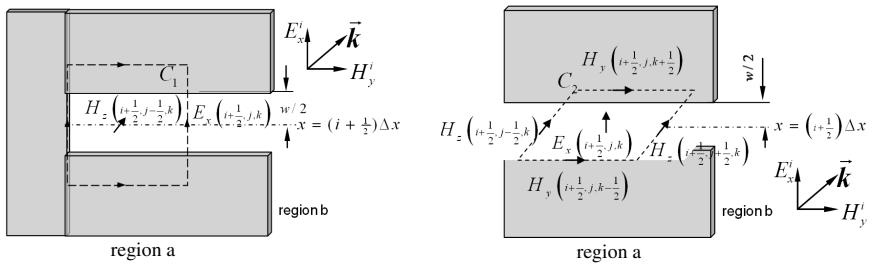

(a) FDTD meshat he slot end edge (b) typical FDTD mesh at the mid of the thin-slot

Figure 4. Typical FDTD mesh near the slot.

4. UPDATING EQUATIONS FOR THE APERTURE COUPLING

To model the slot coupling, the two loops (C_1, C_2) in Fig. 4 derives special attention. The loop C_1 is at the slot end edge, passes the nodes E_x, and surrounds the aperture magnetic field H_z. The loop C_2 penetrates the aperture, passes the nodes H_y and H_z, and surrounds the aperture electric field E_x. It worth to note that the contour path C_1, which is located at the plane $k\Delta_z$, is at the center of the aperture depth.

Firstly, the Faraday's law

$$\frac{\partial}{\partial t}\iint \mathbf{H}\cdot d\mathbf{s} = -\frac{1}{\mu}\oint \mathbf{E}\cdot d\mathbf{l} \tag{22}$$

is applied to the loop C_1. The integrand of the right term in Eq. (22)

is identically zero in the conductor areas, because it is an E-field tangent to a conducting surface. Considering the dramatically varying distribution of the field component H_z at the end cell of the slot [26], the updating equation for H_z derived from (22) can be written as

$$\begin{aligned} & H_z^{n+\frac{1}{2}}\left(i+\frac{1}{2},j+\frac{1}{2},k\right) \\ = \; & H_z^{n-\frac{1}{2}}\left(i+\frac{1}{2},j+\frac{1}{2},k\right)+\frac{\Delta t}{\kappa_{Hz}^{xy}\mu_0\Delta_y}E_x^n\left(i+\frac{1}{2},j+1,k\right) \end{aligned} \tag{23}$$

where κ_{Hz}^{xy} is defined in (21), and n stands for the time steps.

Secondly, we apply the Ampere's law

$$\iint_S \frac{\partial E_x}{\partial t}d\mathbf{s} = -\frac{1}{\varepsilon}\oint \mathbf{H}\cdot d\mathbf{l} \tag{24}$$

to the loop C_2, where E_x and H_y are assumed to be slowly varying along y [18], while E_x and H_z vary rapidly with z. Therefore, (24) can be converted to

$$\begin{aligned} & \Delta_y \int_{-\Delta_z/2}^{\Delta_z/2} \frac{\partial E_x\left(i+\frac{1}{2},j,z\right)}{\partial t}dz \\ = & -\frac{1}{\varepsilon}\begin{bmatrix} \int_{-\Delta_z/2}^{\Delta_z/2}\left(H_z\left(i+\frac{1}{2},j+\frac{1}{2},z\right)-H_z\left(i+\frac{1}{2},j-\frac{1}{2},z\right)\right)dz \\ -\Delta_y\left(H_y\left(i+\frac{1}{2},j,k+\frac{1}{2}\right)-H_y\left(i+\frac{1}{2},j,k-\frac{1}{2}\right)\right) \end{bmatrix} \end{aligned} \tag{25}$$

Substituting (17) and (18) with (19) and (20) into (25), the updating equation for the E_x in the slot can derived

$$\begin{aligned} E_x^{n+1}\left(i+\frac{1}{2},j,k\right) = & E_x^n\left(i+\frac{1}{2},j,k\right)-\frac{1}{\gamma_e}\int_{k\Delta z-\Delta z/2}^{k\Delta z-d/2} E^s dz \\ & +\frac{\Delta t}{\varepsilon_0\Delta_y\gamma_e}\begin{bmatrix} \gamma_m\left(H_z^{n+\frac{1}{2}}\left(i+\frac{1}{2},j+\frac{1}{2},k\right)-H_z^{n+\frac{1}{2}}\left(i+\frac{1}{2},j-\frac{1}{2},k\right)\right) \\ -\Delta_y\left(H_y^{n+\frac{1}{2}}\left(i+\frac{1}{2},j,k+\frac{1}{2}\right)-H_y^{n-\frac{1}{2}}\left(i+\frac{1}{2},j,k-\frac{1}{2}\right)\right) \end{bmatrix} \end{aligned} \tag{26}$$

Here

$$\begin{aligned} \gamma_e = & \kappa_{Ex}^z d+\frac{\nu w}{2}\ln\left[\frac{\Delta_z-d}{\nu w}+\sqrt{1+\left(\frac{\Delta_z-d}{\nu w}\right)^2}\right] \\ & \frac{\left[E_x^h\left(i+\frac{1}{2},j,k-d/2\Delta_z^h\right)+E_x^h\left(i+\frac{1}{2},j,k+d/2\Delta_z^h\right)\right]}{E_x^h\left(i+\frac{1}{2},j,k\right)} \end{aligned} \tag{27}$$

$$\gamma_m = \kappa_{Hz}^z d + \frac{\nu w}{2} \ln \left[\frac{\Delta_z - d}{\nu w} + \sqrt{1 + \left(\frac{\Delta_z - d}{\nu w} \right)^2} \right] \frac{\left[H_z^h \left(i+\frac{1}{2}, j+\frac{1}{2}, k-d/2\Delta_z^h \right) + H_z^h \left(i+\frac{1}{2}, j+\frac{1}{2}, k+d/2\Delta_z^h \right) \right]}{H_z^h \left(i+\frac{1}{2}, j+\frac{1}{2}, k \right)} \quad (28)$$

where κ_{Ex}^z and κ_{Hz}^z are defined in (19) and (20) respectively.

Using the approximation

$$E_x^{n+\frac{1}{2}} \left(i+\frac{1}{2}, j, k \pm 1 \right) = \frac{1}{2} \left[E_x^n \left(i+\frac{1}{2}, j, k \pm 1 \right) + E_x^{n+1} \left(i+\frac{1}{2}, j, k \pm 1 \right) \right] \quad (29)$$

and then the updating Eq. (26) can be written as

$$\begin{aligned} E_x^{n+1} \left(i+\frac{1}{2}, j, k \right) &= E_x^n \left(i+\frac{1}{2}, j, k \right) \\ &+ \frac{\Delta t}{\varepsilon_0 \Delta_y} \left[\begin{array}{l} \frac{\gamma_m}{\gamma_e} \left(H_z^{n+\frac{1}{2}} \left(i+\frac{1}{2}, j+\frac{1}{2}, k \right) - H_z^{n+\frac{1}{2}} \left(i+\frac{1}{2}, j-\frac{1}{2}, k \right) \right) \\ -\frac{\Delta_y}{\gamma_e} \left(H_y^{n+\frac{1}{2}} \left(i+\frac{1}{2}, j, k+\frac{1}{2} \right) - H_y^{n-\frac{1}{2}} \left(i+\frac{1}{2}, j, k-\frac{1}{2} \right) \right) \end{array} \right] \\ &- \frac{1}{8} \frac{(\Delta_z - d)^2}{\gamma_e (\Delta_z - d/2)} \left[\begin{array}{l} \left(E_x^{n+1} \left(i+\frac{1}{2}, j, k-1 \right) - E_x^{n+1} \left(i+\frac{1}{2}, j, k+1 \right) \right) \\ - \left(E_x^n \left(i+\frac{1}{2}, j, k-1 \right) - E_x^n \left(i+\frac{1}{2}, j, k+1 \right) \right) \end{array} \right] \end{aligned} \quad (30)$$

For other field components, Taflove's uniform TSF can be used [20].

5. NUMERICAL RESULTS

Based on the formulation described in the previous section, programs are written to model the aperture coupling. To verify the validity of the proposed method, we checked both the field distribution and the coupling of two apertures. Firstly, the accuracy of the field distribution is checked. Then, the coupling of an aperture located in an infinite plane is modeled, and the waveform of the penetrating electric field is checked. Thirdly, the shielding effectiveness of a rectangular enclosure with a thin-slot predicted by the proposed method is also compared with the measurement result. Care was taken for these examples so that the slot size and the reference point were the same for all methods.

It is agreed that the standard FDTD simulation with a sufficient slot resolution will be sufficiently accurate to be considered as a reference. Therefore, a high-resolution FDTD simulation of the completely computational domain is also carried out to provide a benchmark for comparison. It is worth to note that the high-resolution standard FDTD of the whole area (entitled FDTD), which is

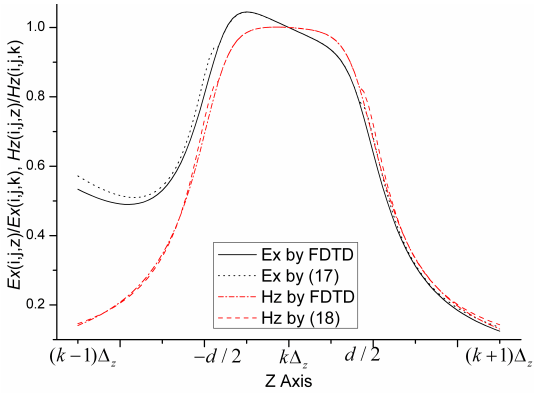

Figure 5. The E_x and H_z distribution near the slot given by the proposed formula and the high-resolution standard FDTD of the whole area (entitled FDTD). The slot size is $w = 1.67\,\text{mm}$, $d = 3.33\,\text{mm}$, $L = 20\,\text{mm}$ in this case.

used as the reference, modeled the completely computational domain. To overcome the memory limit of a serial processor, the parallel implementation is used [27–30]. The convolution PML is used to truncate the computational domain in this work [31–33].

Firstly, to check the precision of the field distributions given in (17) and (18), we compared the field components given by the proposed formula with that given by the high-resolution standard FDTD simulation of the whole computational domain, as shown in Fig. 5. It can be seen that the proposed formalisms are good approximations of the field distributions near the slot. The mean absolute percentage error is 2% and 0.9% for (17) and (18) respectively.

Secondly, the coupling of a thin-slot located in an infinite plane is examined. The aperture size is $w = 1\,\text{mm}$, $d = 2\,\text{mm}$, $L = 20\,\text{mm}$. Both the HTSA and the proposed method are employed to model the aperture coupling. The source is the same as (1), and the penetrating electric field component E_x^p is monitored at the middle point of the reference plane 45 mm away from the slot plane on the shadow side.

In this example, cubic FDTD cells are used for the HTSA, the proposed method and the high-resolution simulation, and the time step is chose to be $\Delta t = \Delta/2c$, where c is the speed of light in the free space. The grid size is 5 mm for the proposed formalism, 2 mm for the HTSA, and 0.033 mm for the high-resolution FDTD. It can be seen from Fig. 6 that both the HTSA and the proposed method are stable, while the proposed method gives a more accurate result than the HTSA. The percentage error of the peak value is 12% and 1.1% for

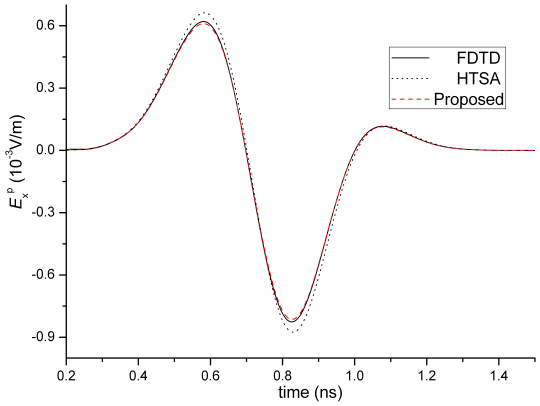

Figure 6. Time-domain responses of a narrow aperture as computed from the hybrid thin-slot algorithm, the proposed method and the high-resolution standard FDTD.

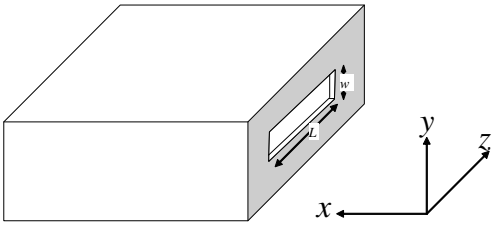

Figure 7. Rectangular enclosure with an aperture located at the center of the front wall.

the HTSA and the proposed method respectively. The time spent for the HTSA is 8.7 seconds, while the proposed method used 1.3 seconds. That is to say, 85% time has saved when the proposed method is used.

Thirdly, we consider a typical rectangular enclosure with dimensions ($300 \times 120 \times 300\,\text{mm}^3$) and a rectangular aperture of size ($100 \times 5\,\text{mm}^2$) located at the center of the right wall, as shown in Fig. 7. The thickness of the enclosure wall is 1.5 mm. The calculated shielding effectiveness is monitored at the center of the enclosure.

The cell size of the local approximation is $0.15 \times 0.33 \times 1.33\,\text{mm}^3$, which results in a $12 \times 15 \times 60$ lattice for the slot area, and the time step is 0.2 ps. A TEM mode Gaussian pulse, $E_y = \exp[-4\pi(t - t_0)^2/\tau^2]$ is used as the incidence pulse of the approximation, where $\tau = 20\,\text{ps}$ and $t_0 = 20\,\text{ps}$. 2500 times step are carried out for the local approximation, which results in a 4 second time usage. Then we can get the coefficients (19)–(21) from the numerical integral, as shown in

Table 1.

Coefficient	κ_{Hz}^{xy}	γ_m (cm)	γ_e (cm)
Value	1.470907	1.0183796	1.0211317

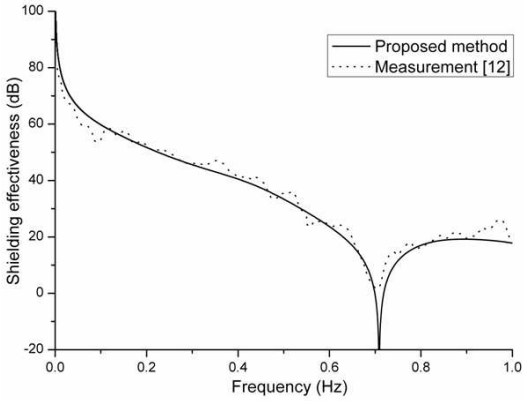

Figure 8. SE versus frequency at the center of the $300\times120\times300\,\mathrm{mm}^3$ enclosure with a $100\times5\,\mathrm{mm}^2$ aperture.

Table 1.

The cell dimension is $25\times24\times25\,\mathrm{mm}^3$ in the x, y and z directions respectively, and the time step is $\Delta t = 80\,\mathrm{ps}$ for the main computation domain of the proposed method. 500000 time steps have been carried out and 168 minutes is used. Since it is difficult for the HTSA to deal with apertures whose width is larger than its depth, he shielding effectiveness of only the proposed method is compared with the measurement of [34].

Figure 8 shows the calculated and measured shielding effectiveness at the center of the enclosure, which shows a good agreement. The mean absolute percentage error is 1.4% for the proposed method when compared with the measurement. Note that much of the variation in the measurement is due to the imperfect damping of resonances in the screened room.

From the numerical analysis above, it can be seen that the proposed method is numerically efficient and stable, and the local approximation is highly efficient while the approximation time can be ignored.

6. CONCLUSIONS

A local approximation method is derived in this work for the FDTD analysis of short apertures with a finite thickness. The major idea of the proposed method is to derive the field distribution near the slot from the equivalence principle together with the high-resolution local approximation.

The equivalence principle is used to decouple the aperture coupling into three parts by placing the equivalent magnetic current sheets on the two sides of the slot. With the high-resolution local approximation, the equivalent magnetic current sheets are obtained with the modified slot width. Then the field near the slot can be derived from the conformal mapping technique and the linear distribution assumption. By casting the field distribution into the contour paths near the slot, the updating equations can be obtained.

To verify the validity of the proposed method, the field distribution and two examples are included. The varying field distribution of the proposed method is verified from the comparison of that from the high-resolution standard FDTD simulation of the completely computational domain. The accuracy of the proposed method has been proved from the comparison of both time domain and frequency domain results. It is demonstrated that the local approximation is highly efficient while timesaving, and the method presented here is stable, numerically and computationally efficient. It is verified that about 85% time has been saved when the proposed method is used, compared with the HTSA.

The proposed method can be applied in the FDTD analysis of short apertures with a finite thickness so that it is not necessary to reduce the FDTD cell size to make concessions to the slot size.

ACKNOWLEDGMENT

This work was supported by the National Natural Science Foundation of China under Grant No. 60971063.

REFERENCES

1. Kong, Y.-D. and Q.-X. Chu, "Reduction of numerical dispersion of the six-stages split-step unconditional-stable FDTD method with controling parameters," *Progress In Electromagnetics Research*, Vol. 122, 175–196, 2012.
2. Lee, K. H., I. Ahmed, R. S. M. Goh, E. H. Khoo, E. P. Li, and T. G. G. Hung, "Implementation of the FDTD method based on lorentz-drude dispersive model on GPU for plasmonics

applications," *Progress In Electromagnetics Research*, Vol. 116, 441–456, 2011.

3. Izadi, M., M. Z. A. Ab Kadir, C. Gomes, and W. F. W. Ahmad, "An analytical second-FDTD method for evaluation of electric and magnetic fields at intermediate distances from lightning channel," *Progress In Electromagnetics Research*, Vol. 110, 329–352, 2010.
4. Xiao, S.-Q., Z. H. Shao, and B.-Z. Wang, "Application of the improved matrix type FDTD method for active antenna analysis," *Progress In Electromagnetics Research*, Vol. 100, 245–263, 2010.
5. Sirenko, K., "An FFT-accelerated FDTD scheme with exact absorbing conditions for characterizing axially symmetric resonant structures," *Progress In Electromagnetics Research*, Vol. 111, 331–364, 2011.
6. Cao, D.-A. and Q.-X. Chu, "FDTD analysis of chiral discontinuities in waveguides," *Progress In Electromagnetics Research Letters*, Vol. 20, 19–26, 2011.
7. Ai, X., Y. Han, C. Y. Li, and X.-W. Shi, "Analysis of dispersion relation of piecewise linear recursive convolution FDTD method for space-varying plasma," *Progress In Electromagnetics Research Letters*, Vol. 22, 83–93, 2011.
8. Silva, A. O., R. Bertholdo, M. G. Schiavetto, B.-H. V. Borges, S. J. L. Ribeiro, Y. Messaddeq, and M. A. Romero, "Comparative analysis between experimental characterization results and numerical FDTD modeling of self-assembled photonic crystals," *Progress In Electromagnetics Research B*, Vol. 23, 329–342, 2010.
9. Koo, V. C., Y. K. Chan, V. Gobi, M. Y. Chua, C. H. Lim, C.-S. Lim, C. C. Thum, T. S. Lim, Z. Bin Ahmad, K. A. Mahmood, M. H. Bin Shahid, C. Y. Ang, W. Q. Tan, P. N. Tan, K. S. Yee, W. G. Cheaw, H. S. Boey, A. L. Choo, and B. C. Sew, "A new unmanned aerial vehicle synthetic aperture radar for environmental monitoring," *Progress In Electromagnetics Research*, Vol. 122, 245–268, 2012.
10. Wounchoum, P., D. Worasawate, C. Phongcharoenpanich, and M. Krairiksh, "A switched-beam antenna using circumferential-slots on a concentric sectoral cylindrical cavity excited by coupling slots," *Progress In Electromagnetics Research*, Vol. 120, 127–141, 2011.
11. Wang, X., M. Zhang, and S.-J. Wang, "Practicability analysis and application of PBG structures on cylindrical conformal microstrip antenna and array," *Progress In Electromagnetics Research*, Vol. 115, 495–507, 2011.
12. Yang, P., F. Yang, and Z.-P. Nie, "DOA estimation with sub-

array divided technique and interpolated esprit algorithm on a cylindrical conformal array antenna," *Progress In Electromagnetics Research*, Vol. 103, 201–216, 2010.

13. Pergol, M. and W. Zieniutycz, "Rectangular microstrip resonator illuminated by normal-incident plane wave," *Progress In Electromagnetics Research*, Vol. 120, 83–97, 2011.
14. Ahdi Rezaeieh, A. and M. Kartal, "A new triple band circularly polarized square slot antenna design with crooked T and F-shape strips for wireless applications," *Progress In Electromagnetics Research*, Vol. 121, 1–18, 2011.
15. Wang, C.-J. and T. H. Lin, "A multi-band meandered slotted-groundplane resonator and its application of low-pass filter," *Progress In Electromagnetics Research*, Vol. 120, 249–262, 2011.
16. Wang, C.-J. and Y. Dai, "Studies of power-combing of open slot antenna arrays," *Progress In Electromagnetics Research*, Vol. 120, 423–437, 2011.
17. Melamed, T., "Pulsed beam expansion of electromagnetic aperture field," *Progress In Electromagnetics Research*, Vol. 114, 317–332, 2011.
18. Xu, K., Z. Fan, D.-Z. Ding, and R.-S. Chen, "Gpu accelerated unconditionally stable Crank-Nicolson FDTD method for the analysis of three-dimensional microwave circuits," *Progress In Electromagnetics Research*, Vol. 102, 381–395, 2010.
19. Li, J., L.-X. Guo, and H. Zeng, "FDTD method investigation on the polarimetric scattering from 2-D rough surface," *Progress In Electromagnetics Research*, Vol. 101, 173–188, 2010.
20. Gilbert, J. and R. Holland, "Implementation of the thin-slot formalism in the finite-difference EMP code THRED II," *IEEE Trans. Nucl. Sci.*, Vol. 28, 4269–4274, Dec. 1981.
21. Taflove, A., K. R. Umashankar, B. Beker, et al., "Detailed FDTD analysis of electromagnetic fields penetrating narrow slots and lapped joint in thick conducting screen," *IEEE Transactions on Antennas and Propagation*, Vol. 36, 247–257, Feb. 1988.
22. Riley, D. J. and C. D. Turner, "Hybrid thin-slot algorithm for the analysis of narrow apertures in finite difference time-domain calculations," *IEEE Transactions on Antennas and Propagation*, Vol. 38, 1943–1950, Dec. 1990.
23. Xiong, R., B. Chen, Q. Yin, and Z.-Y. Cai, "Improved formalism for the FDTD analysis of thin-slot penetration by equivalence principle," *IEEE Antennas and Wireless Propagation Letters*, Vol. 10, 655–657, 2011.

24. Ma, K.-P., M. Li, J. L. Drewniak, T. H. Hubing, and T. P. V. Doren, "Comparison of FDTD algorithms for subcellular modeling of slots in shielding enclosures," *IEEE Trans. Electromagnetic Compatiblity*, Vol. 39, 147–155, May 1997.
25. Harrington, R. F., *Time Harmonic Electromagnetic Fields*, McGraw-Hill, New York, 1961.
26. Xiong, R., B. Chen, Q. Yin, and B. H. Zhou, "The capacitance thin-slot formalism revisited: An alternative expression for the thin-slot penetration," *Journal of Electromagnetic Waves and Applications*, Vol. 26, No. 4, 446–458, 2012.
27. Lei, J. Z., C. H. Liang, and Y. Zhang, "Study on shielding effectiveness of metallic cavities with apertures by combining parallel FDTD method with windowing technique," *Progress In Electromagnetics Research*, Vol. 74, 85–112, 2007.
28. Vaccari, A., A. Cala' Lesina, L. Cristoforetti, and R. Pontalti, "Parallel implementation of a 3-D subgridding FDTD algorithm for large simulation," *Progress In Electromagnetics Research*, Vol. 120, 263–292, 2011.
29. Taboada, J. M., M. G. Araujo, J. M. Bertolo, L. Landesa, F. Obelleiro, and J. L. Rodriguez, "MLFMA-FFT parallel algorithm for the solution of large-scale problems in electromagnetics," *Progress In Electromagnetics Research*, Vol. 105, 15–30, 2010.
30. Ergul, O., "Parallel implementation of MLFMA for homgeneous objects with various material properties," *Progress In Electromagnetics Research*, Vol. 121, 505–520, 2010.
31. Roden, J. A. and S. D. Gedney, "Convolution PML (CPML): An efficient FDTD implementation of the CFS-PML for arbitrary media," *Microwave and Optical Technology Letters*, Vol. 27, No. 5, 334–339, Dec. 2000.
32. Cai, Z.-Y., B. Chen, Q. Yin, and R. Xiong, "The WLP-FDTD method for periodic structures with oblique incident wave," *IEEE Transactions on Antennas and Propagation*, Vol. 59, 3780–3785, 2011.
33. Mao, Y.-F., B. Chen, H.-Q. Liu, J.-L. Xia, and J.-Z. Tang, "A hybrid implicit-explicit spectral FDTD scheme for the oblique incidence programs on periodic structures," *Progress In Electromagnetics Research*, Vol. 128, 153–170, 2012.
34. Robinson, M. P., T. M. Benson, C. Christopoulos, J. F. Dawson, M. D. Ganley, A. C. Marvin, S. J. Porter, and D. W. P. Thomas, "Analytical formulation for the shielding effectiveness of enclosures with apertures," *IEEE Trans. Electromagnetic Compatibility*, Vol. 40, No. 3, 240–247, Aug. 1998.